Correlation functions of hadron currents in the QCD vacuum calculated in lattice QCD

M.-C. Chu
W.K. Kellogg Radiation Laboratory California Institute of Technology, 106-38 Pasadena, California 91125

J. M. Grandy
T-8 Group, MS B-285, Los Alamos National Laboratory, Los Alamos, New Mexico 87545

S. Huang
Department of Physics, FM-15, University of Washington, Seattle, Washington 98195

J. W. Negele
Center for Theoretical Physics, Laboratory for Nuclear Science and Department of Physics, Massachusetts Institute of Technology, Cambridge, Massachusetts 02139
(Received 1 June 1993)

Point-to-point vacuum correlation functions for spatially separated hadron currents are calculated in quenched lattice QCD on a $16^3 \times 24$ lattice with $6/g^2 = 5.7$. The lattice data are analyzed in terms of dispersion relations, which enable us to extract physical information from small distances where asymptotic freedom is apparent to large distances where the hadronic resonances dominate. In the pseudoscalar, vector, and axial vector channels where experimental data or phenomenological information are available, semiquantitative agreement is obtained. In the nucleon and Δ channels, where no experimental data exist, our lattice data complement experiments. Comparison with approximations based on sum rules and interacting instantons are made, and technical details of the lattice calculation are described.

PACS number(s): 12.38.Gc

I. INTRODUCTION

The structure of the QCD vacuum and of hadrons poses an exceedingly rich and complicated many-body problem. Hence, as with other many-body systems, it is instructive to focus ones attention on appropriately selected ground state correlation functions, to calculate their properties quantitatively, and to understand their behavior physically.

The correlation functions we address in this work are the spacelike-separated correlation functions of hadron currents in the QCD vacuum which have recently been discussed in an extensive review by Shuryak [1]. For example, in the case of a meson current $J(x) \equiv \bar{q}(x)\Gamma q(x)$, we consider the correlation function $\langle\Omega|TJ(x)\bar{J}(0)|\Omega\rangle$ where x is spacelike and for simplicity may be taken to be purely spatial so that the two currents are at equal time and $|\Omega\rangle$ denotes the interacting ground state. This correlation function has a number of appealing features. In many channels, it has been determined phenomenologically by using dispersion relations to relate it to e^+e^- hadron production and τ-decay experimental data. Because it is defined at equal time (or Euclidean time), it may be calculated on the lattice and in the interacting instanton approximation as well as by using sum rules. It complements bound state hadron properties in the same way scattering phase shifts provide information about the nucleon-nucleon force complementary to that provided by the properties of the deuteron. Just as nucleon-nucleon scattering allows one to explore the spin-spin, spin-orbit, and tensor components of the nuclear force at different spatial separation in much more detail than deuteron observables which reflect the composite effect of all channels and ranges, so also the interaction or "scattering" of virtual quarks and antiquarks from meson sources at different spatial separations allows one to obtain much more detailed information about quark interactions for different channels and spatial separations than the composite effects reflected in hadron bound states.

Much of the richness of the study of these correlation functions arises from the different physics involved at different spatial separations. For convenience, we will consider the ratio of the physical correlation functions to those of massless noninteracting quarks, which by dimensional considerations must fall as x^{-6}. By asymptotic freedom, at extremely short distances the interactions between quarks must become negligible, and the ratio approaches 1. For slightly larger distances, where interactions are small but non-negligible, one should be able to use the leading terms in the Wilson operator product expansion to describe the deviation from unity. In the absence of separate, exact evaluation of the relevant operators, one must use the factorization approximations which have been developed in connection with sum rule techniques, and we will see below that these approximations are successful in some channels and fail in oth-

ers. At still larger distances, the full complexity of nonperturbative QCD comes into play, and one may use this region to test and refine QCD motivated models such as the interacting instanton approximation. For example, a dominant feature of instanton models is the 't Hooft effective interaction which couples left- and right-handed quarks and thus in leading order contributes only to the scalar and pseudoscalar channels and with opposite sign. Finally, at very large separation, the decay of the correlation functions is governed by the lightest hadron mass in the relevant channel.

As a result of this diverse range of physics at different spatial separations, it is clear that definitive lattice calculations of correlation functions would provide an exceedingly useful supplement to accessible experimental data in allowing one to quantitatively explore and improve approximations based on the operator produce expansion, sum rules, and interacting instantons. We view the exploratory calculation described in this work as a successful first step in this direction. Although the lattice size, lattice spacing, statistics, extrapolation to the physical pion mass, and quenched approximation limit our present accuracy, the semiquantitative agreement we obtain in channels for which experimental data exist and the lack of major pathologies in statistical noise or extrapolation to the chiral limit clearly indicate the potential for lattice calculation of these correlation functions. In addition to the meson correlation functions discussed above, we will also address analogous correlation functions for baryon currents.

The outline for this paper is as follows. In Sec. II we define the hadron currents we use, present the results for correlation functions of these currents for free quarks on the lattice, and describe a useful phenomenological parametrization in terms of resonance and continuum contributions. The lattice calculation is described in Sec. III, including the treatment of lattice anisotropies, corrections for images, extrapolation in κ, and determination of parameters of the phenomenological fits. Section IV presents the results. For each meson and baryon channel, the lattice correlation functions extrapolated to the physical pion mass are presented and, where possible, compared with correlation functions extracted from experimental data and approximations based on sum rules and instanton approximations. In addition, masses, coupling constants, and thresholds extracted from phenomenological fits to the lattice results are also presented and discussed. Our conclusions are discussed in Sec. V.

II. CORRELATION FUNCTIONS

The two-point function for a generic current J is defined as the vacuum expectation value of the time-ordered product

$$\langle\Omega|TJ(x)\bar{J}(0)|\Omega\rangle \equiv R(x)\,. \tag{2.1}$$

For a local field theory, the two-point function in momentum space can be uniquely characterized up to a polynomial by its absorptive part through a dispersion relation

$$\int d^4x e^{iqx}\langle\Omega|TJ(x)\bar{J}(0)|\Omega\rangle = K(q)\int ds\frac{f(s)}{s-q^2-i\epsilon}+P(q^2)\,, \tag{2.2}$$

where $K(q)$ is a kinematic factor which only depends on the quantum numbers of J, and $P(q^2)$ is a finite-order polynomial of q^2.

In the case of free massless quarks, without the gauge interaction, the spectral density function $f(s)$ can be calculated easily. For a mesonic channel with current J composed of quark and antiquark operators and Dirac and flavor matrices tabulated in Table I, the corresponding $f(s)$ is simply given by the imaginary part of the fermion bubble graph in the same channel. Up to an overall sign, $f(s) = 3s/8\pi^2$ and $K(q) = 1$ for scalar and pseudoscalar channels. Similarly $f(s) = 1/4\pi^2$ and $K(q) = q^2 g_{\mu\nu} - q_\mu q_\nu$ for vector and axial vector channels. For convenience, we contract indices μ and ν in vector and axial channels to obtain direction independent correlators.

To calculate free baryonic correlators with massless quarks, it is more convenient to work in coordinate space, rather than in momentum space. Otherwise, we would have to calculate the imaginary parts of two-loop graphs.

TABLE I. Hadron currents and correlation functions.

Channel	Current	Correlator $R(x)$	$f_0(s)$
Vector	$J_\mu = \bar{u}\gamma_\mu d$	$\langle\Omega\|TJ_\mu(x)\bar{J}_\mu(0)\|\Omega\rangle$	$1/(4\pi^2)$
Axial	$J^5_\mu = \bar{u}\gamma_\mu\gamma_5 d$	$\langle\Omega\|TJ^5_\mu(x)\bar{J}^5_\mu(0)\|\Omega\rangle$	$1/(4\pi^2)$
Pseudoscalar	$J^p = \bar{u}\gamma_5 d$	$\langle\Omega\|TJ^p(x)\bar{J}^p(0)\|\Omega\rangle$	$3s/(8\pi^2)$
Scalar	$J^s = \bar{u}d$	$\langle\Omega\|TJ^s(x)\bar{J}^s(0)\|\Omega\rangle$	$3s/(8\pi^2)$
Nucleon	$J^N = \epsilon_{abc}[u^a C\gamma_\mu u^b]\gamma_\mu\gamma_5 d^c$	$\frac{1}{4}\mathrm{Tr}[\langle\Omega\|TJ^N(x)\bar{J}^N(0)\|\Omega\rangle x_\nu\gamma_\nu]$	$s^2/(64\pi^4)$
Δ	$J^\Delta_\mu = \epsilon_{abc}[u^a C\gamma_\mu u^b]u^c$	$\frac{1}{4}\mathrm{Tr}[\langle\Omega\|TJ^\Delta_\mu(x)\bar{J}^\Delta_\mu(0)\|\Omega\rangle x_\nu\gamma_\nu]$	$3s^2/(256\pi^4)$

In coordinate space, a massless quark propagator has the simple form

$$\langle 0|Tq(x)\bar{q}(0)|0\rangle = \frac{i}{2\pi^2}\frac{x_\mu\gamma^\mu}{x^4}. \tag{2.3}$$

For the nucleon and Δ currents defined in Table I, it is easy to verify the following:

$$\langle 0|TJ^N(x)\bar{J}^N(0)|0\rangle = i\frac{24}{\pi^6}\frac{x_\mu\gamma^\mu}{x^{10}}, \tag{2.4}$$

$$\langle 0|TJ^\Delta_\mu(x)\bar{J}^\Delta_\mu(0)|0\rangle = -i\frac{18}{\pi^6}\frac{x_\mu\gamma^\mu}{x^{10}}. \tag{2.5}$$

If quarks are given small masses, there will be terms proportional to the identity in Dirac space with coefficients linear in quark masses. In order to have stable and quark mass insensitive free correlators, which will be used as the normalizations for the interacting correlators, we multiply these baryonic correlators by a factor of $x_\mu\gamma^\mu$ and then take the trace in the Dirac indices. Finally, a Fourier transform is necessary to obtain the spectral density functions.

In order to divide out the lattice artifacts at small distances, the corresponding noninteracting lattice correlators have been used for normalization. A small quark mass has to be introduced to render the lattice quark propagator well defined. It can be verified that a finite quark mass only affects the propagator at distances larger than the Compton wavelength. For a quark mass of the order of 50 MeV, significant deviation from the massless continuum quark propagator only occurs at distances beyond 4 fm. At distances less than 2 fm, the deviation is at most a few percent, as discussed below.

Once the gauge interaction is turned on, we do not in general know how to calculate the spectral density functions. However, we do know their qualitative behavior, based on experimental information and general properties of local field theories. So the natural strategy is to parametrize the spectral density functions phenomenologically and then determine the parameters by fitting them to lattice results. For the present application, it is adequate to use the parametrization

$$f(s) = \lambda^2\delta(s-M^2) + f_c(s)\theta(s-s_0), \tag{2.6}$$

where M is the bound state mass, λ denotes the coupling of the current to the bound state, and s_0 is the threshold for the onset of a continuum contribution $f_c(s)$. Note that in this parametrization, sharp resonances are treated as pole terms, while broad and overlapping resonances are treated as a continuum. The functional form of $f_c(s)$ is in general very complicated. Because of asymptotic freedom, we expect that $f_c(s)$ approaches the free result $f_0(s)$ for sufficiently large s, and for intermediate s the noninteracting result could be corrected perturbatively. However, since the threshold $\sqrt{s_0}$ is around 1.5–2.0 GeV, which is still in the nonperturbative region, there is no analytical means to accurately describe all detailed behavior near threshold. Hence, we will parametrize $f_c(s)$ by the functional form of the free result $f_0(s)$, listed also in Table I, throughout the whole continuum region, and treat the threshold s_0 as a phenomenological parameter which produces the correct integrated strength for the low s nonperturbative region of the spectral function. Note that, as a result, the value of s_0 need not correspond precisely to the threshold for the first excited state found in the particle data tables.

A sketch of a generic spectral function and its representation by the parametrization of Eq. (2.6) with $f_0(s)$ are shown in Fig. 1(a) by the light and heavy curves, respectively. The single isolated resonance is represented by a δ-function at M^2. We have chosen the case of a scalar or pseudoscalar channel, where the noninteracting continuum spectral function grows linearly in s. One observes that the linear curve $f_0(s)$ joins the continuum smoothly at large s and with the value of s_0 shown, includes roughly the same strength as the full continuum curve at low s.

The same kind of approximation is widely used in QCD sum rule calculations. It should be emphasized that using $f_0(s)$ to approximate $f_c(s)$ is consistent with the lattice approximation, since the resonance parameters and continuum strength near threshold are determined by physics well below the lattice cutoff $p^2 = (\pi/a)^2 \approx 9$ GeV^2. This is in contrast with the operator product expansion based QCD sum rule calculations, in which there may not be an appropriate region to match the theoretical calculations and the phenomenological results.

Given the spectral density described above, Eq. (2.6), an inverse Fourier transform of Eq. (2.2) defines the phenomenological correlators in coordinate space as a function of M, λ, and s_0. Note that the polynomial $P(q^2)$ only contributes at the point $x = 0$ and can be ignored

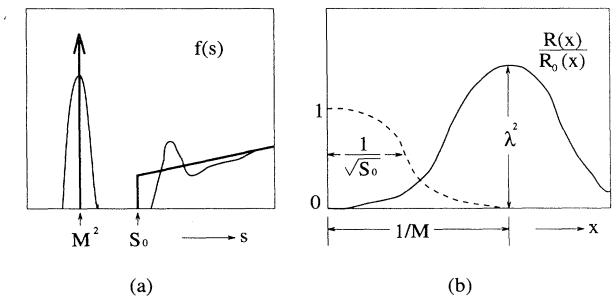

FIG. 1. Sketch of generic spectral function and its Fourier transform. The light solid curves in the left panel (a) show a typical spectral function as a function of the mass squared, s, comprising an isolated resonance and a region of broad overlapping resonances merging with the continuum. The heavy lines show the parametrization, Eq. (2.6), where the isolated resonance is represented by a δ function at M^2 with strength λ^2 and the continuum is parametrized by $f_0(s)$ for the noninteracting system (in this case linear in s) with a cutoff s_0. The right panel (b) shows the coordinate space Fourier transform of the parametrized spectral function. The resonance δ function produces the broad solid curve whose position is proportional to M^{-1} with height proportional to λ^2. The continuum term produces the dashed curve which is normalized to one at the origin with extent proportional to $s_0^{-\frac{1}{2}}$.

at finite x. In doing the Fourier transform the following two integrals are used:

$$\int \frac{d^4q}{(2\pi)^4} e^{-iqx} \frac{i}{q^2 - s} = \frac{\sqrt{s}}{4\pi^2 x} K_1(\sqrt{s}x) \tag{2.7}$$

and

$$\int \frac{d^4q}{(2\pi)^4} e^{-iqx} \frac{q^\mu \gamma_\mu}{q^2 - s} = \frac{x_\mu \gamma^\mu}{4\pi^2 x^2} s K_2(\sqrt{s}x) \tag{2.8}$$

for spacelike x. In practice we always normalize $R(x)$ by the corresponding free correlator with massless quarks, $R_0(x)$,

$$R_0^{\text{meson}}(x) = \frac{1}{x} \int_0^\infty ds\, f_0^{\text{meson}}(s) \sqrt{s} K_1(\sqrt{s}x) \sim \frac{1}{x^6} \tag{2.9}$$

and

$$R_0^{\text{baryon}}(x) = \int_0^\infty ds\, f_0^{\text{baryon}}(s) s K_2(\sqrt{s}x) \sim \frac{1}{x^8} . \tag{2.10}$$

An analogous normalization is also done for the lattice data, as described more specifically in the next section.

In Fig. 1(b) we sketch the corresponding two-point function in coordinate space, normalized by the free correlators with massless quarks. To distinguish the physics in difference regions, we plot the resonance and continuum contributions separately. Because of asymptotic freedom, the continuum piece, denoted by the dashed line, starts at 1 and then gradually decays to zero with its width characterized by $\sim 1/\sqrt{s_0}$. In contrast, the resonance starts as a power of x at small x and reaches its maximum at around $\sim 1/M$ with a height proportional to λ^2. Although the full correlation function is the sum of these two contributions, it is important to note that both in this example and in many of the physical calculations it is possible to distinguish the resonance and continuum contributions to a large extent and thereby understand the physical origin of the numerical results.

For later convenience we list all the spectral functions and their corresponding parametrized correlators.

In the vector channel

$$f^V(s) = 3\lambda_\rho^2 \delta(s - M_\rho^2) + \frac{3s}{4\pi^2} \theta(s - s_0) , \tag{2.11}$$

$$R^V(x)/R_0^V(x) = \frac{\pi^2}{8} \left(\frac{\lambda_\rho}{M_\rho^2} \right)^2 (M_\rho x)^5 K_1(M_\rho x) + \frac{1}{16} \int_{\sqrt{s_0}x}^\infty d\alpha\, \alpha^4 K_1(\alpha) . \tag{2.12}$$

The factor of 3 in front of λ_ρ^2 is due to contraction of indices μ, ν from $q^2 g_{\mu\nu} - q_\mu q_\nu$.

In the axial vector channel

$$f^A(s) = 3\lambda_{A_1}^2 \delta(s - M_{A_1}^2) - f_\pi^2 M_\pi^2 \delta(s - M_\pi^2) + \frac{3s}{4\pi^2} \theta(s - s_0) , \tag{2.13}$$

$$R^A(x)/R_0^A(x) = \frac{\pi^2}{8} \left(\frac{\lambda_{A_1}}{M_{A_1}^2} \right)^2 (M_{A_1} x)^5 K_1(M_{A_1} x) - \frac{\pi^2}{24} \left(\frac{f_\pi}{M_\pi} \right)^2 (M_\pi x)^5 K_1(M_\pi x) + \frac{1}{16} \int_{\sqrt{s_0}x}^\infty d\alpha\, \alpha^4 K_1(\alpha) . \tag{2.14}$$

In this channel there are two invariants, $q^2 g_{\mu\nu} - q_\mu q_\nu$ and $q_\mu q_\nu$, which have independent spectral functions; the first includes the A_1 pole and the second includes the pion pole. The relative minus sign between the A_1 and π pole terms, arising from kinematics, explains why the correlator in this channel becomes negative at very large distances. The continuum contributions from the two invariants have the same asymptotic form and are expressed as a single term.

In the pseudoscalar channel

$$f^P(s) = \lambda_\pi^2 \delta(s - M_\pi^2) + \frac{3s}{8\pi^2} \theta(s - s_0) , \tag{2.15}$$

$$R^P(x)/R_0^P(x) = \frac{\pi^2}{12} \left(\frac{\lambda_\pi}{M_\pi^2} \right)^2 (M_\pi x)^5 K_1(M_\pi x) + \frac{1}{16} \int_{\sqrt{s_0}x}^\infty d\alpha\, \alpha^4 K_1(\alpha) . \tag{2.16}$$

In the scalar (isovector) channel

$$f^S(s) = \frac{3s}{8\pi^2} \theta(s - s_0) , \tag{2.17}$$

$$R^S(x)/R_0^S(x) = \frac{1}{16} \int_{\sqrt{s_0}x}^\infty d\alpha\, \alpha^4 K_1(\alpha) . \tag{2.18}$$

Since there is no known resonance in this channel, only the continuum part is included in the spectral function.

In the nucleon channel

$$f^N(s) = q_\mu \gamma^\mu \left[\lambda_N^2 \delta(s - M_N^2) + \frac{s^2}{64\pi^4} \theta(s - s_0) \right] + \cdots , \tag{2.19}$$

where the ellipsis represents terms with other Dirac structure and

$$R^N(x)/R_0^N(x) = \frac{\pi^4}{96} \left(\frac{\lambda_N}{M_N^3} \right)^2 (M_N x)^8 K_2(M_N x) + \frac{1}{3072} \int_{\sqrt{s_0}x}^{\infty} d\alpha \, \alpha^7 K_2(\alpha) . \tag{2.20}$$

In the Δ channel,

$$f^\Delta(s) = q_\mu \gamma^\mu \left[2\lambda_\Delta^2 \delta(s - M_\Delta^2) + \frac{3s^2}{256\pi^4} \theta(s - s_0) \right] + \cdots , \tag{2.21}$$

where again the ellipsis stands for terms with other Dirac structure and

$$R^\Delta(x)/R_0^\Delta(x) = \frac{\pi^4}{36} \left(\frac{\lambda_\Delta}{M_\Delta^3} \right)^2 (M_\Delta x)^8 K_2(M_\Delta x) + \frac{1}{3072} \int_{\sqrt{s_0}x}^{\infty} d\alpha \, \alpha^7 K_2(\alpha) . \tag{2.22}$$

The factor of 2 in front of λ_Δ^2 comes from $g_{\mu\nu}$ multiplying the Rarita-Schwinger tensor:

$$\left[g_{\mu\nu} - \frac{1}{3}\gamma_\mu\gamma_\nu + \frac{1}{3}(\gamma_\mu q_\nu - \gamma_\nu q_\mu) - \frac{2}{3}\frac{q_\mu q_\nu}{M_\Delta^2} \right] ,$$

with $q^2 = M_\Delta^2$.

Because the local currents we have used are not conserved on the lattice, we need, in principle, to know the relevant finite renormalization factors before we can assign a definite meaning to the fitted values of λ. Although in the mesonic channels these renormalization factors were estimated in some cases in the literature [2], there are no similar estimates in the baryonic channels, as far as we know. To circumvent this problem, we have fitted the pole term relative to the continuum term and ignored the overall normalization. As long as the currents are multiplicatively renormalized, which we assume, this scheme should be a good way to avoid the explicit renormalization factors. The primary limitation is that, due to the relatively poor knowledge of the continuum contribution $f_c(s)$, we introduce a systematic error when we approximate $f_c(s)$ by $f_0(s)$. However, we do not expect the systematic error to be too large, since $f_c(s)$ does not have pronounced peaks near the threshold. Ultimately, a consistency check should be made with other fitting schemes.

III. LATTICE CALCULATION

The lattice calculations were performed on a $16^3 \times 24$ lattice in the quenched approximation with Wilson fermions at an inverse coupling $6/g^2 = 5.7$, corresponding to a physical lattice spacing defined by the proton mass of approximately $a = 0.17$ fm. Lattice spacings defined by the string tension or the rho mass would be 15% higher or lower, respectively. The motivation for using such a large coupling, which is crude by current standards, is the fact that the necessary propagators for point sources were available from Soni and co-workers [3], while propagators for larger lattices and a correspondingly larger inverse coupling constant are normally calculated from distributed sources to optimize the overlap with hadronic wave functions and are thus unsuitable for the current application. This inverse coupling constant is large enough to give a semiquantitative approximation and has allowed us to make a thorough study of the finite lattice effects described below. Point propagators for 16 configurations were used for five values of the hopping parameter, $\kappa = 0.154, 0.160, 0.164, 0.166$, and 0.168. To think about these propagators in physical units, it is convenient to associate a quark mass $m_q \equiv (1/2\kappa - 1/2\kappa_c)\, a^{-1}$ with each value of κ, where $\kappa_c = 0.1692$, yielding the five values of m_q, 317, 199, 110, 67, and 25 MeV, respectively. Extrapolation to the value of κ which reproduces the pion mass then corresponds to extrapolation to $m_q = 5.2$ MeV. Because the quark propagators had hard-wall boundary conditions in the time direction, all correlation functions were calculated on the central time slice containing the source. Finite size effects in the spatial direction are discussed below. In order to calculate the ratio of interacting to free correlation functions, corresponding free quark lattice propagators were calculated for $m_q a = 0.05$ on a $(48)^4$ lattice, which was sufficiently large to eliminate finite volume effects for spatial separation less than 4 fm. The effect of the small quark mass m_q was estimated in the continuum by evaluating the ratio of noninteracting quark correlation functions $\langle J\bar{J}\rangle|_m / \langle J\bar{J}\rangle|_0$, with the result that the finite mass overestimated the ratio at $x/a = 5$ by factors ranging from the smallest value of 0.3% in the vector channel to the largest value of 5.5% in the axial channel. Preliminary analysis of the same lattice calculation has been reported in Ref. [4].

A. Lattice anisotropy

In order to obtain a physical approximation to the continuum correlation functions, it is necessary to understand and correct for all relevant lattice artifacts. A

particularly important lattice effect for the present application is the anisotropy introduced into the rotationally invariant continuum correlation functions by the Cartesian lattice.

The effect and a means for dealing with it are clearly displayed for the case of noninteracting quarks on the lattice. In the hopping-parameter expansion, it is clear that points in Cartesian directions can be reached with fewer steps than equidistant points in other directions. Although at very large separations entropy effects should favor wiggly paths which approach the continuum result in all directions, one clearly expects propagators and thus correlation functions to be larger than the continuum result for points near the Cartesian axes, and for this effect to become more pronounced at short distances. These expectations are clearly borne out in the case of the vector meson correlation functions shown in Fig. 2. The solid line in the upper curve denotes the continuum result for noninteracting quarks. All discrete lattice results have been calculated on the central time slice (to avoid complications from hard-wall boundary conditions) and averaged over equivalent permutations of the axes, so we will denote sites by (n_x, n_y, n_z) with $n_x \geq n_y \geq n_z$. By the previous argument, the Cartesian sites $(n, 0, 0)$ should lie furthest above the continuum, and as shown by the diamonds in the figure, these points indeed do lie the highest. The diagonal directions (n, n, n) should suffer least from the lattice artifacts, and we observe that these points, denoted by circles, do approximate the continuum well throughout. The subdiagonal direction $(n, n, 0)$ denoted by squares, is intermediate between the two extremes.

By asymptotic freedom, one would expect the QCD solution on the lattice to approximate the free solution at short distances, and one observes from the lower curve in the top portion of Fig. 2 that the qualitative structure of the QCD solution, including its spatial anisotropies, is remarkably similar to the free case plotted above it. Note that for clarity, statistical error bars have been omitted but are comparable to the symbol size. We therefore have every reason to believe that the diagonal sites should give a good approximation to the continuum, and furthermore that much of the anisotropy will in fact cancel out when we calculate the ratio of the QCD correlation function to the free correlation function.

The ratio of the QCD to free correlation functions is plotted in the lower section of Fig. 2. Here, the error bars, which are still omitted for clarity, are typically of the order of 2% at $x/a = 5$ and 15% at $x/a = 10$. In principle one would like to normalize the ratios at an infinitesimally small separation. Although in Fig. 2 we arbitrarily normalized the data at the closest point (0,0,1), since we have argued that the diagonal points are most reliable, we have normalized all our subsequent physical results at the first nonzero diagonal separation $(1, 1, 1)$, corresponding to a physical separation of ~ 0.29 fm. Note for future reference that we are considering the ratio of quantities which separately are varying over 6 orders of magnitude. As one would expect, at small x, the lattice anisotropy is nearly identical in the interacting and free case so that the ratio is nearly isotropic. At intermediate distances $x/a \sim 5$, the cancellation is not complete, but an order of magnitude effect in the QCD correlation function is reduced to a 50% effect in the ratio. In this respect the vector case we show in Fig. 2 is a worst case, and most other channels have much greater cancellation. At large x, the anisotropy becomes negligible in both numerator and denominator. In order to increase the statistics, while maintaining a good approximation to the continuum, we have adopted a prescription of including not only the diagonal sites $\mathbf{d} \equiv (n, n, n)$ denoted

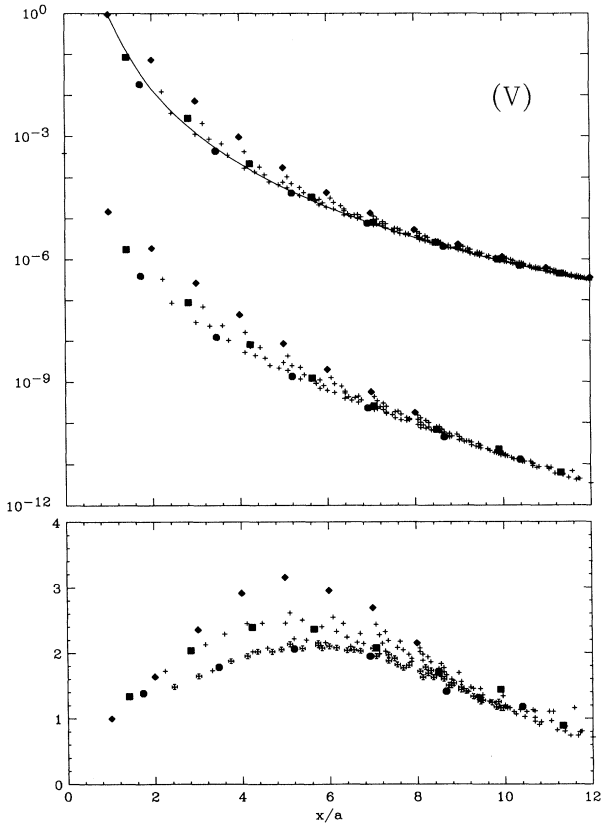

FIG. 2. Vector meson correlation functions. The upper curve shows the correlation function for noninteracting massless quarks calculated in the continuum (solid curve) and lattice results for $ma = 0.05$. Diamonds denote the Cartesian directions $(n, 0, 0)$, squares denote the directions $(n, n, 0)$, circles denote the diagonal directions (n, n, n), and the crosses denote all other points. The lower curve in the upper panel shows the corresponding lattice results for interacting quarks with $m_q = 110$ MeV, shifted by an arbitrary normalization factor. There is no longer an exact continuum curve, but all other symbols have the same meaning and clearly show the similarity of lattice artifacts in the free and interacting cases. The lower panel shows the ratio of interacting to free correlation functions normalized to 1 at the first point, where the circles, squares, and diamonds denote the same lattice directions as above. The fancy crosses denote all other lattice points lying within a cone of opening angle 26° surrounding the diagonal directions. The smooth solid curve defined by these fancy crosses and the circles represents the physical ratio of correlation functions.

by the circles, but also all sites $\mathbf{r} = (n_x, n_y, n_z)$ such that $\hat{\mathbf{r}} \cdot \hat{\mathbf{d}} \geq 0.9$. That is, we include all sites falling within a cone surrounding the diagonal with opening angle $\theta = \arccos(0.9) \approx 26°$. The rationale for this prescription is that propagators to these points sample the same general class of quark paths as the diagonal points, and one observes that the fancy crosses in Fig. 2 denoting these sites indeed define a smooth curve which includes the circles representing the pure diagonal points.

The behavior shown in Fig. 2 is representative of all the meson and baryon channels we have calculated. In particular, data measured within the 26° cone surrounding the diagonal always lie on a universal curve for all channels and the anisotropy associated with the Cartesian directions is smaller in all other channels. The analogous correlation functions for nucleon currents are shown in Fig. 3, where all the symbols and plots are defined as in Fig. 2. The primary difference with respect to the meson case arises from the fact that the correlation functions contain three quark propagators and include the contraction $\gamma_\mu x^\mu$ so that the free case falls like x^{-8} instead of x^{-6}. The anisotropies have the same behavior as before, are extremely similar in the interacting and noninteracting case, and cancel out even more completely than before in the ratio. The locus of points specified by circles and fancy crosses again defines a smooth curve

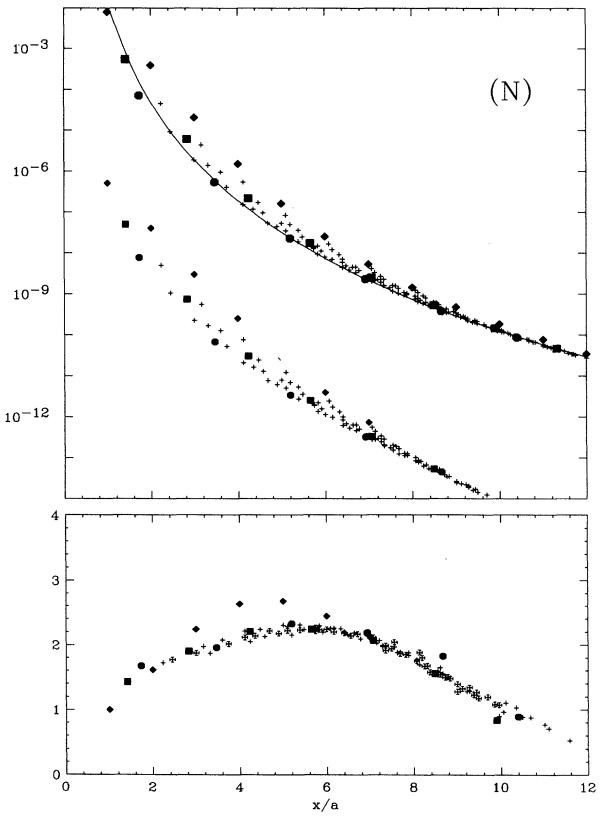

FIG. 3. Nucleon correlation functions. All quantities are defined as in Fig. 2.

which we believe to be a good physical approximation to the continuum.

B. Image corrections

Because of periodic boundary conditions for quarks at the spatial boundaries, the large distance behavior of quark propagators is affected by the presence of image sources in adjacent unit cells. The correction for images in correlation functions of the form considered in this work is discussed in detail in Refs. [5,6]. The main point is that because $\langle \Omega \left| J(x)\bar{J}(0) \right| \Omega \rangle$ involves a gauge-invariant closed loop of propagators, any cross terms in which the contraction of one propagator involves different fundamental and image currents than the other propagator necessarily has the topology of a Wilson line encircling the entire lattice and thus is negligible in the confining phase. Hence, only diagonal terms involving images occur, and the effect of all first images is to yield the desired infinite volume correlation function summed over all first image sources. Special symmetry points may be corrected trivially. For example the center of a face of the unit cell $\left(\frac{N}{2}, 0, 0\right)$, where N is the linear dimension of the unit cell (16 in our case), is equidistant from two sources and the correlation function at this point is thus multiplied by 1/2. Similarly, the center of an edge $\left(\frac{N}{2}, \frac{N}{2}, 0\right)$ is equidistant from four sources yielding a factor 1/4, and the corner $\left(\frac{N}{2}, \frac{N}{2}, \frac{N}{2}\right)$ is equidistant from eight sources yielding a factor of 1/8. For all other points, one must numerically subtract the image contributions, which is done iteratively by approximately correcting for images using an appropriately defined parametric curve, least squares fitting the parameters to the corrected data, and iterating to self-consistency. In practice, this procedure always yields a smooth universal curve at large distances for the cases of interest here, and the lattice QCD data in Fig. 2 and Fig. 3 have been corrected in this way.

C. Extrapolation

Because it is impractical to calculate quark propagators at a quark mass light enough to produce a physical pion, it is necessary to perform a sequence of calculations at a series of heavier quark masses and extrapolate to the quark mass corresponding to the physical pion mass. Nearby lattice data are grouped in bins of $n \leq x < n + 1$ lattice spacings, and data within each bin are combined to a single value by means of a statistically weighted average, with each correlator datum y_i given a weight $w_i = 1/\sigma_i^2$, where σ_i is the statistical uncertainty of the datum. In the pseudoscalar channel, where the fits are particularly sensitive to the abscissas, we determine these abscissas by the statistically weighted average. In all other channels, the abscissas of the binned data are approximated by the central values $n + 0.5$. The binned data at each separation, computed from the lightest four quark masses enumerated above, are extrapolated using a least squares quadratic fit. In the pseudoscalar channel we extrapolate the logarithm of the correlator, and in the

other channels the correlator itself is extrapolated.

The extrapolation of the correlator in the pseudoscalar channel is displayed in Fig. 4. In this channel, the height of the resonance peak diverges as λ_π^2/M_π^4 and the position of the peak also diverges as $1/M_\pi$. Despite these difficulties, we believe that we have performed our calculations over a sufficient range of quark masses to obtain a reasonable picture of the pion correlator at the physical pion mass since the plot shows that our extrapolation is indeed smooth. The pseudoscalar channel is the worst case of the extrapolation; the other channels contain no Goldstone bosons, and consequently the extrapolations are well behaved in the chiral limit.

We have shown the extrapolation as a function of the quark mass in all the channels for two typical separations in Fig. 5. This figure shows that the data at a given current separation vary smoothly as a function of quark mass. A quadratic fit to all five data points gives a reasonable description of the mass dependence over a range of 300 MeV, and the quadratic fit to the lowest four masses used for the actual extrapolation is seen to provide an excellent fit to all the data. Thus we have confidence in the extrapolation of the correlators from heavier quark masses to the quark mass corresponding to the physical pion mass.

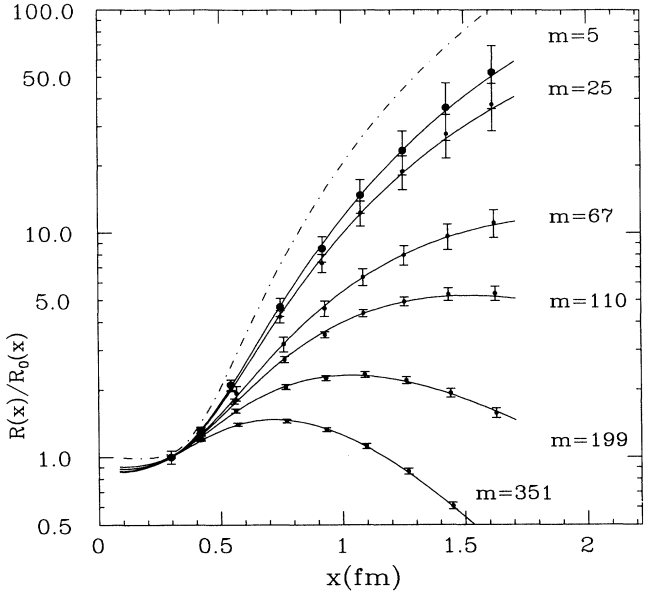

FIG. 4. Quark mass dependence of pseudoscalar correlation function. Open circles denote binned lattice data at five values of the quark mass. Extrapolation to the quark mass 5.2 MeV, which corresponds to the physical pion mass, yields the points denoted by solid dots with the associated statistical errors. The solid lines are three-parameter fits to the data, and the dot-dashed line indicates the phenomenological result of Ref. [1].

D. Fitting with phenomenological spectral function

The hadronic current correlators for the six channels shown in Table I, which have been computed for all geometrically independent separations near the body diagonal and combined into bins of one lattice unit of separation, are fitted using the dispersion forms based on the phenomenological spectral functions described in Sec. II. Where possible, we have minimized χ^2 with respect to all four parameters: the arbitrary normalization, the resonance mass M, the coupling λ of the current to the resonance, and the continuum threshold s_0. As described below, in some channels the lattice data do not allow us to freely fit all four parameters so we fix some of the parameters to values independently known from previous lattice calculations or phenomenology. In the axial channel there are two additional parameters associated with the pion resonance term, f_π and M_π, and the fit is performed by allowing three of the six available parameters to vary in the minimization of χ^2. As noted previously, we set the lattice spacing to $a = 0.17\,\mathrm{fm}$ using the well-established value for the proton mass [7,6], with which our fitted proton mass is consistent.

Using this fitting procedure, we extract the physical parameters of the spectral functions. The resonance masses, M, which are the energies of the lowest eigenstates with the quantum numbers of the current, will be shown to be consistent with the masses measured accurately by the asymptotic decay of two-point functions at large time separations [7,6]. From the ratio of the resonance to continuum terms, we directly determine the physical coupling constants which can be compared with experimental data and the values used in existing models and sum rule calculations. As discussed previously, the threshold s_0 does not correspond precisely to the first excited state in the data tables since it parametrizes the integrated strength in the low energy region of the continuum. In the graphs presented below, the correlators are normalized to one at the separation $\sqrt{3}a = 0.29$ fm.

E. Error analysis

The lattice correlator measurements at different current separations at a given quark mass are highly correlated, particularly at large separations, and we compute the errors in the binned data directly using the single elimination jackknife method. In the quadratic extrapolation to the quark mass $m_q = 5.2\,\mathrm{MeV}$, the uncertainty in the extrapolated values is taken to be the range of the values for which χ^2 changes by less than one. Correlations between data for different quark masses are not included in the calculation of the standard deviations of the extrapolated data so it is possible that these statistical uncertainties are underestimated. Unfortunately, even with binned data, the correlation matrix is so poorly conditioned that the fitted parameters for the phenomenological spectral function have to be determined neglecting the correlations between the binned data points. The valley of χ^2 in parameter space is in general rather complicated, and for several channels and quark masses two nearby minima of χ^2 occur in parameter space. Hence,

we search directly for the range in each fitted parameter for which a fit can be found that increases χ^2 by less than one from the minimum value. This search is accomplished by repeatedly fixing one of the parameters in which χ^2 is minimized and finding the minimum χ^2 in the space of the remaining parameters. In general the statistical range of each parameter is not symmetric about its best fitted value, and we present optimal values and asymmetric ranges for the fitted physical parameters.

IV. RESULTS

This section presents the results of our lattice calculations, their parametrization in terms of the resonance and continuum spectral functions described in Sec. II, and comparisons with phenomenological analyses of experimental data and theoretical calculations based on QCD sum rules and instanton models. The principal results for correlation functions are presented in Figs. 6–8 and the fitted parameters are tabulated in Table II. We will present and discuss the results channel by channel.

A. Vector channel (ρ)

The results for the vector channel are shown in the upper portion of Fig. 6, and provide a good example of a successful four-parameter fit to the lattice results. As is evident from the figure, the continuum term, denoted by the long dashes, and the resonance term, denoted by the dotted curve, are separately well determined and the sum fits the lattice data, denoted by solid circles, quite well.

The ρ mass extracted from this fit agrees well with the mass measured from the exponential decay of the two-point function in Euclidean time [7]. This agreement between the resonance mass determined by the intermediate-range behavior of the correlation function and the asymptotic decay, which occurs systematically in all the channels we have investigated and is a significant test of the consistency of the parametrization of the spectral density, will be discussed subsequently in connection with Fig. 9. As is well known, however, at $\beta = 5.7$ the ρ mass on the lattice is lighter than the experimental mass. As shown in Table II, both the values

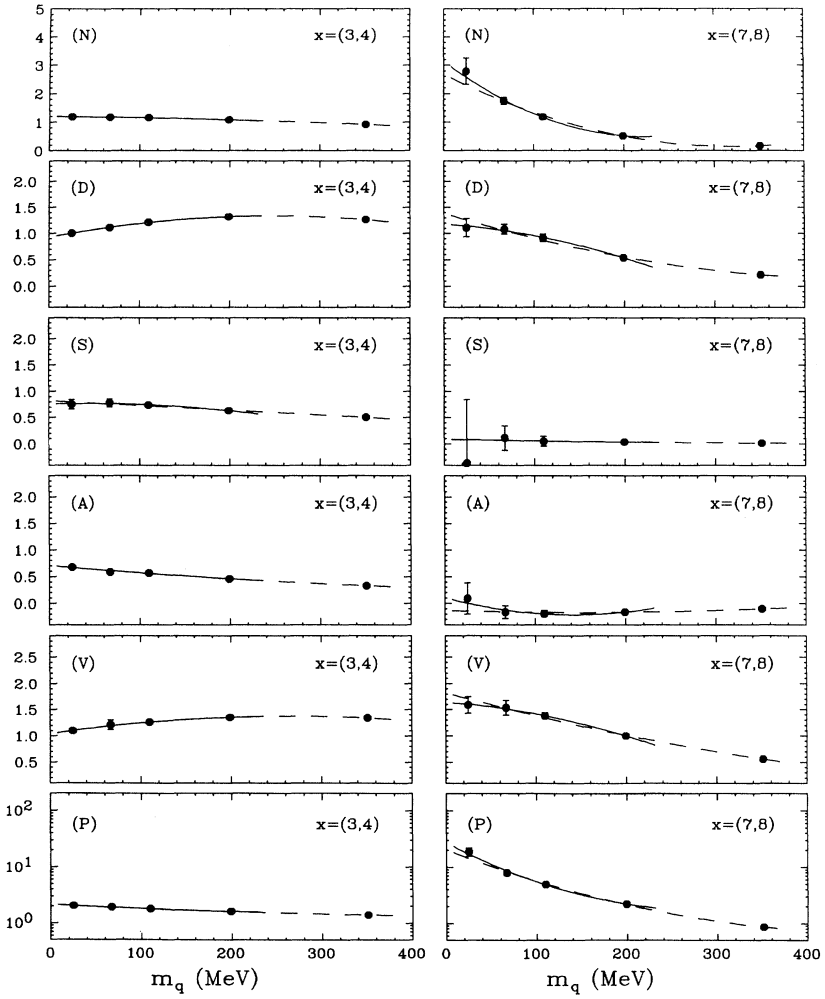

FIG. 5. Extrapolation of correlation functions in the quark mass for nucleon (N), Δ (D), scalar (S), axial (A), vector (V), and pseudoscalar (P) channels. Binned lattice data for x in the intervals of 3–4 lattice units and 7–8 lattice units are shown as a function of the quark mass in MeV. Where error bars are not visible, they are smaller than the dot size. Quadratic least squares fits to the last four and five data points are shown by solid and dashed lines, respectively.

of the coupling constant λ and the threshold s_0 are close to the phenomenological values.

The lattice result for the vector correlation function is reasonably close to the phenomenological result obtained by Shuryak [1] from a dispersion analysis of $e^+e^- \rightarrow$even number of π's. The fact that the phenomenological result lies below the lattice result follows from the fact that resonance peak scales as λ^2/M_ρ^4 and the lattice mass lies below experiment while the coupling constant agrees with the phenomenological value. The result of the instanton model is qualitatively similar, although lower than phenomenology.

The most salient physics result in this channel is the fact that although the free correlator falls by 4 orders of magnitude, the ratio of the interacting to non-interacting correlators remains close to one. Although the ratio must approach unity very close to $x = 0$ by asymptotic freedom and there is no leading order 't Hooft instanton induced interaction in this channel, the ratio remains close to unity for much larger distances than any simple arguments suggest. This feature, which has been called superduality, arises in this work as a "conspiracy" of the parameters of the resonance and continuum terms of the spectral function.

B. Pseudoscalar channel (π)

The pseudoscalar channel exhibits the most dramatic dependence on the quark mass, reflecting the special role of the pion as a Goldstone boson. In this case, the extrapolation is slightly sensitive to the fact we extrapolated the log of the correlator, and logarithmic extrapolation in x as well would give a slightly higher result.

The successful four-parameter fit shown in the lower panel of Fig. 6 provides strong support for our method of determining the resonance and continuum terms. Note

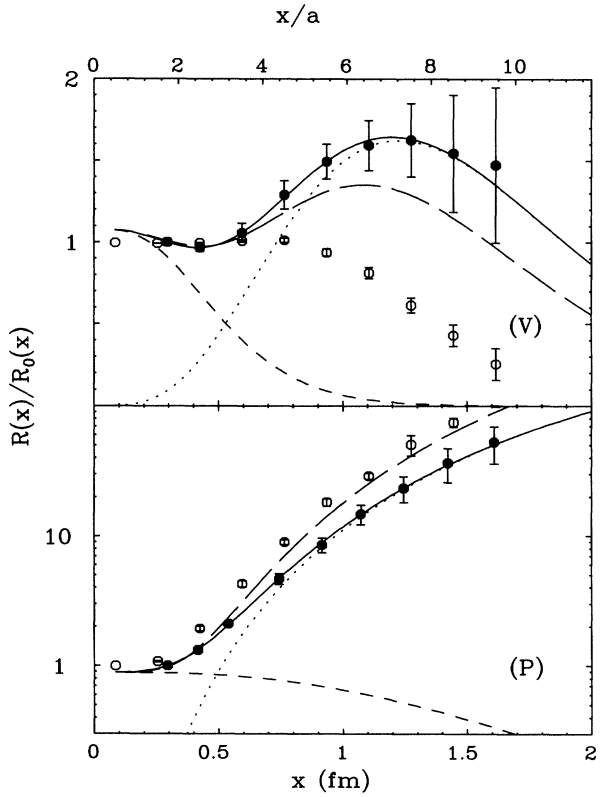

FIG. 6. Vector (V) and pseudoscalar (P) correlation functions are shown in the upper and lower panels, respectively. Extrapolated lattice data are denoted by the solid points with error bars. Fits to the lattice data using the phenomenological form discussed in the text are given by the solid curves, with the continuum and resonance components denoted by short-dashed and dotted curves, respectively. The empirical results determined by dispersion analysis of experimental data in Ref. [1] are shown by the long-dashed curves. The open circles denote the results of the random instanton vacuum model of Ref. [8].

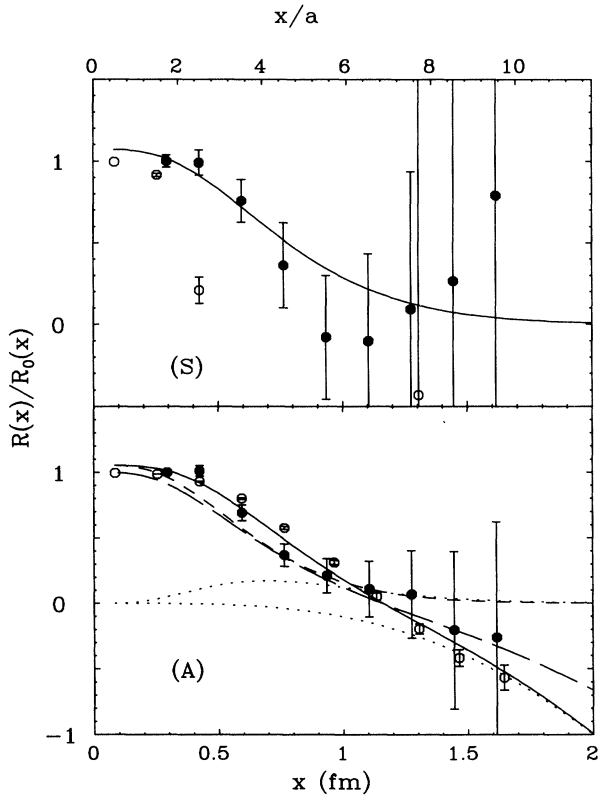

FIG. 7. Scalar (S) and axial vector (A) correlation functions are shown in the upper and lower panels, respectively. Extrapolated lattice data and empirical results from dispersion analysis of experimental data are given by solid dots and long dashes as in Fig. 6. The results of the random instanton vacuum model are denoted by open circles which have been shifted slightly to the right where necessary for clarity. The fit to the scalar lattice data includes only a continuum term, denoted by the solid curve. The fit to the axial lattice data includes A_1 and π resonance terms of opposite signs, denoted by the dotted curves as well as the short-dashed continuum curve, yielding the total result given by the solid curve.

that because of the light pion mass, the peak of the resonance occurs far outside of the range in which the data is fit. Nevertheless, the extracted mass and coupling constant agree well with the empirical results. Because of the overlap of the resonance and continuum regions, the threshold $\sqrt{s_0}$ is not fully determined. Rather, we only obtain a bound of 1.0 GeV by the criterion that χ^2 increase by at most 1. The fact that this is somewhat below the first excited state is consistent with the fact that it must represent the integrated strength included in the peaks of low-lying resonances.

As already noted in connection with Fig. 4, the lattice result is close to the phenomenological result from the dispersion analysis of Ref. [1]. It is also quite close to the results of the random instanton vacuum model [8] and consequently the parameters in Table II agree well. Physically, this is the most attractive channel and the leading order 't Hooft interaction is attractive in it.

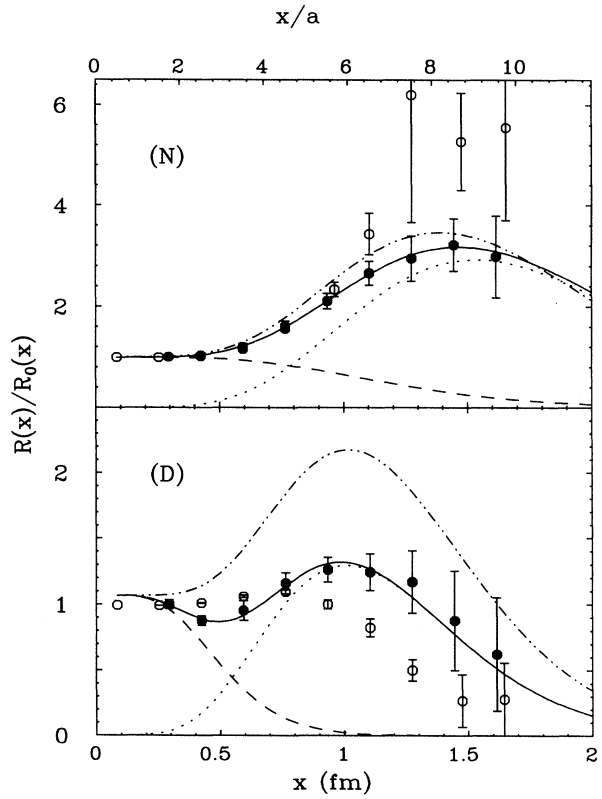

FIG. 8. Nucleon (N) and Δ (D) correlation functions are shown in the upper and lower panels, respectively. As in Fig. 6, extrapolated lattice data are denoted by solid dots, the phenomenological fit is given by the solid curve with continuum and resonance components given by dashed and dotted curves, respectively. The results of the random instanton model are given by the open circles, again shifted slightly where necessary for clarity. The results from the QCD sum rule calculation of Ref. [9] are indicated by the double-dot-dashed lines.

C. Scalar channel

The results in the scalar channel are shown in the upper panel of Fig. 7. By the general dispersion analysis, the correlator should be non-negative in this channel, and one observes that the lattice results fall rapidly to zero at roughly 1 fm, albeit with large errors at large distances. There is no evidence for resonances, either experimentally or in the lattice calculation, and the results are fit adequately by the continuum term with a single threshold parameter.

Physically, since the 't Hooft interaction produces a repulsive interaction from instantons to leading order, one expects a rapid falloff. However, the lattice results fall off much more slowly than the random instanton vacuum model as shown in Fig 7. The overall behavior in the scalar channel is consistent with that of two noninteracting "very massive" quarks.

D. Axial vector channel (A_1)

The axial vector channel is unique in that it is the only channel for which the general dispersion analysis does not restrict the spectral function to be positive. As shown in Eqs. (2.13) and (2.14), the axial and pseudoscalar contributions enter with opposite sign, so we expect resonance terms of opposite sign in addition to the continuum contribution. As expected, one indeed observes that the lattice data in the lower panel of Fig. 7 go negative at large distances. Although one may wonder about the statistical significance given the large error bars from extrapolation, the negativity is unambiguous in the lattice measurements at each unextrapolated quark mass (see for example the axial channel data at $x = 7.5$ in Fig. 5). Because the data are insufficient to determine six parameters, we fixed the masses of π and A_1, specified the coupling of A_1 to be the same as the ρ, and fit the norm, threshold, and pion coupling.

In this channel, the extrapolated lattice result agrees quite well with the phenomenological result derived partly from experimental τ-decay data [1] and with the results of the random instanton vacuum model [8].

E. Nucleon channel

The results for the nucleon channel are shown in the upper panel of Fig. 8. In this case the lattice data have relatively small error bars, and we obtain a good fit yielding the correct nucleon mass. The fit is relatively insensitive to the threshold s_0, and the fit shown in the figure is performed with $\sqrt{s_0} = 1.2$ GeV. The upper bound of 1.4 GeV in Table II is determined by the highest value for which χ^2 is increased by less than 1. In connection with Fig. 5, one should note that, with the exception of the pseudoscalar channel, the nucleon correlator has the strongest quark mass dependence of any channel.

One observes that the lattice results are quite consistent with the sum rule result of Ref. [9], shown by the

TABLE II. Fitted parameters.

Channel	Source	M (GeV)	λ	$\sqrt{s_0}$ (GeV)
Vector	Lattice	0.72 ± 0.06	$(0.41 \pm 0.02$ GeV$)^2$	1.62 ± 0.23
	Instanton[a]	0.95 ± 0.10	$(0.39 \pm 0.02$ GeV$)^2$	1.50 ± 0.10
	Phenomenology[b]	0.78	$(0.409 \pm 0.005$ GeV$)^2$	1.59 ± 0.02
Pseudoscalar	Lattice	0.156 ± 0.01	$(0.44 \pm 0.01$ GeV$)^2$	< 1.0
	Instanton[a]	0.142 ± 0.014	$(0.51 \pm 0.02$ GeV$)^2$	1.36 ± 0.10
	Phenomenology[b]	0.138	$(0.480$ GeV$)^2$	1.30 ± 0.10
Nucleon	Lattice	0.95 ± 0.05	$(0.293 \pm 0.015$ GeV$)^3$	< 1.4
	Instanton[a]	0.96 ± 0.03	$(0.317 \pm 0.004$ GeV$)^3$	1.92 ± 0.05
	Sum rule[c]	1.02 ± 0.12	$(0.324 \pm 0.016$ GeV$)^3$	1.5
	Phenomenology[b]	0.939	?	1.44 ± 0.04
Δ	Lattice	1.43 ± 0.08	$(0.326 \pm 0.020$ GeV$)^3$	3.21 ± 0.34
	Instanton[a]	1.44 ± 0.07	$(0.321 \pm 0.016$ GeV$)^3$	1.96 ± 0.10
	Sum rule[c]	1.37 ± 0.12	$(0.337 \pm 0.014$ GeV$)^3$	2.1
	Phenomenology[b]	1.232	?	1.96 ± 0.10

[a]Instanton liquid model [8].
[b]Phenomenology estimated by Shuryak [1] and from the particle data book [10].
[c]QCD sum rule by Belyaev and Ioffe [9].

double-dot-dashed curve. In addition, although there are substantial statistical errors at large distance, the random instanton vacuum model is also close to the lattice results [8].

F. Δ channel

The results in the Δ channel are shown in the lower panel of Fig. 8. In this case, we obtain a good four-parameter fit, with well-determined continuum and resonance contributions shown in the figure. The mass is slightly higher than the APE result, and will be discussed in connection with Fig. 9 below. The coupling constant is consistent with the value determined from the sum rule.

The results of the random instanton vacuum model are qualitatively similar, but do not display as pronounced a resonance term and also fall off more rapidly at large distance. In plotting the sum rule result in this channel, denoted by the double-dot-dashed line, we have used the mass determined from the sum rule analysis itself, rather than the experimental mass, to make the theory internally consistent. This has the effect of reducing the height of the resonance peak somewhat from Ref. [1]. Note that in the trace we have calculated for our correlator given in Table II, there are spin-$\frac{1}{2}$ contaminants, so one should not expect complete agreement with the sum rule result. To the extent that excited states are heavy, the effect of these contaminants should not be too large.

G. Mass dependence of parameters

Having discussed the parameters characterizing the spectral function for the fits to extrapolated lattice data in each channel, it is useful to observe the dependence of these parameters on the quark mass. Hence, we have fit the correlators calculated for each quark mass, and summarized the results in Figs. 9 and 10.

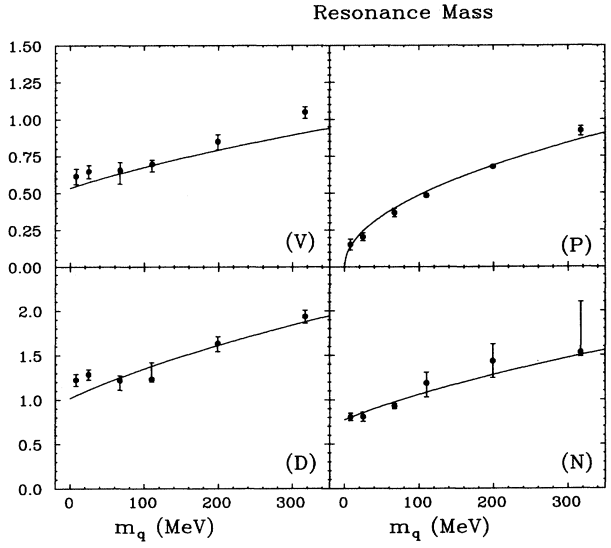

FIG. 9. Comparison of the masses extracted from the resonance term in the spectral function, denoted by solid points with error bars, with masses determined from the asymptotic decay of two-point functions by the APE Collaboration [7], shown by the solid curves. The systematic agreement as a function of quark mass m_q in the vector (V), pseudoscalar (P), Δ (D), and nucleon (N) channels is a significant consistency check of the present analysis.

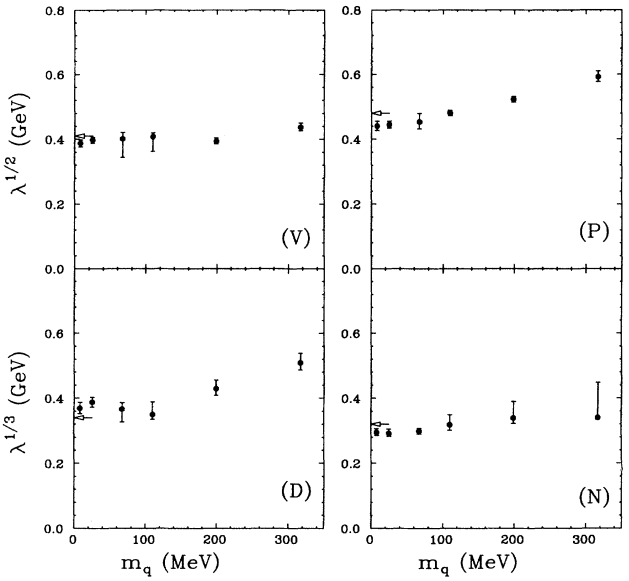

FIG. 10. Dependence of the coupling constant λ for the resonance term on the quark mass, m_q , in the vector (V), pseudoscalar (P), Δ (D), and nucleon (N) channels. The five data points to the right indicate lattice measurements which clearly extrapolate smoothly to the chiral limit. The left point denotes the results extrapolated to $m_q = 5.2$ MeV, the quark mass corresponding to the physical pion. Note that these results compare well with the phenomenological results denoted by the arrows for the vector and pseudoscalar channels and with the sum rule results denoted by the arrows for the nucleon and Δ channels.

Figure 9 shows the resonance mass as a function of quark mass for the vector, pseudoscalar, Δ, and nucleon channels. For comparison, the mass dependence determined by the APE Collaboration [7] from extremely accurate measurements of the exponential decay of two-point functions at large time separations is also shown by the solid curves. The detailed agreement between the fits to the resonance masses and the APE results is striking and provides a strong confirmation of the consistency and effectiveness of the parametrization and fitting procedure. The agreement of the pion mass is particularly significant, since the peak of the resonance is not even contained in the region of the fit. One statistical fluke worth noting is the fact that the Δ mass is slightly high at $m_q = 25$ MeV, which also carries over into a high value for the extrapolated data.

Figure 10 shows comparable mass dependence for the coupling constants. Although there is no smooth reference curve in this case, one observes that the coupling constants vary quite smoothly with the quark mass, so that there is nothing pathological happening in the chiral limit. For reference, the experimental or model results from Table II are denoted by arrows at the physical pion mass.

V. CONCLUSIONS

In summary, we believe these results demonstrate the feasibility and utility of lattice calculations of these vacuum correlation functions and of the phenomenological analysis of the results.

Even for the relatively large lattice spacing in this work, we have understood and controlled the lattice artifacts associated with the finite volume and anisotropy of the lattice. For those channels in which empirical results are available from dispersion analysis of experimental data, we have shown that our results are in semiquantitative agreement with experiment.

The phenomenological analysis of the lattice results in terms of a four-parameter characterization of the spectral function has been shown to be successful in parametrizing the data and in understanding its physical content. The analysis has been shown to be reliable in the sense that the fit parameters are systematically consistent with other lattice measurements of masses and with phenomenology.

These results strongly motivate more definitive calculations on larger lattices with $6/g^2 = 6$. Having established the reliability of lattice results in channels for which experimental data exist, we may then use the lattice calculation as a tool to study correlation functions in channels in which experimental measurement are not feasible or are unavailable. In addition, it is instructive to perform companion calculations with cooled configurations in which the contributions of instantons alone can be compared with the full lattice results and instanton based models. Work in these directions is in progress.

ACKNOWLEDGMENTS

It is a pleasure to thank Edward Shuryak for extensive discussions on many aspects of this work and for making data available to us prior to publication. We wish to acknowledge a helpful discussion with Boris Ioffe concerning application of sum rules to the Δ channel. We also thank Amarjit Soni for making his point propagators available to us, and the National Energy Supercomputer Center for providing Cray-2 computer resources. This work was supported in part by funds provided by the U.S. Department of Energy (DOE) under Contract Nos. DE-AC02-76ER03069 and DE-FG06-88ER40427, and the National Science Foundation under Grant No. PHY 88-17296.

[1] E. Shuryak, Rev. Mod. Phys. **65**, 1 (1993).
[2] G. Martinelli, C. T. Sachrajda, and A. Vladikas, Nucl. Phys. **B358**, 212 (1991).
[3] A. Soni, Ntl. Energy Res. Supercomput. Center Buffer **14**, 23 (1990); C. Bernard, T. Draper, G. Hockney, and A. Soni, Phys. Rev. D **38**, 3540 (1988).
[4] M.-C. Chu, J. M. Grandy, S. Huang, and J. W. Negele, Phys. Rev. Lett. **70**, 225 (1993).

[5] M. Burkardt, J. M. Grandy, and J. W. Negele, MIT Report No. CTP#2108, 1993 (unpublished).
[6] J. M. Grandy, Ph.D. thesis, Massachusetts Institute of Technology, 1992.
[7] The APE Collaboration, P. Bacilieri *et al.* Nucl. Phys. **B317**, 509 (1989).
[8] E. V. Shuryak and J. J. M. Verbaarschot, "Mesonic Correlation Functions in the Random Instanton Vacuum," Stony Brook Report No. SUNY-NTG-92-40, 1992 (unpublished); T. Schäfer, E. V. Shuryak, and J. J. M. Verbaarschot, "Baryonic Correlators in the Random Instanton Vacuum," Stony Brook Report No. SUNY-NTG 92-45 1993 (unpublished).
[9] B. L. Ioffe, Nucl. Phys. **B188**, 317 (1981); V. M. Belyaev and B. L. Ioffe, Zh. Eksp. Teor. Fiz. **83**, 976 (1982) [Sov. Phys. JETP **56**, 547 (1982)].
[10] Particle Data Group, K. Hikasa *et al.,* Phys. Rev. D **45**, S1 (1992).